18

A Three-Dimensional Numerical Simulation of the Free Surface Flow Around a Ship Hull

J. B. V. Wanderley, M. Vitola, S. H. Sphaier and C. Levi
LabOceano – COPPE/UFRJ
Brazil

1. Introduction

Offshore oil and gas production is advancing fast towards water depth deeper and deeper. In the last couple of years, offshore oil production depth world records have been successively superseded. Oil industry is about to achieve production in fields approaching 2000m water depth while keeping on exploring new oil reservoirs in ocean depths close to 3000m. As water depth increases, the distance from oil field to mainland depots increases at similar rates and more hostile the ocean environment becomes. In such operational conditions the use of VLCC ship tanker, as a production unit, has been proved to be technically and economically appealing.

Good hydrodynamic characteristics in severe sea environments, adequate storage capability and possibly the low prices of used tanker hulls in the ship market are the main reasons to justify the increasing popularity of tanker hull as production units (Floating Storage and Offloading – FSO and Floating Production Storage and Offloading – FPSO) among offshore oil producer companies. The complete assessment of the dynamic behavior of moored tankers depends very much on the accuracy of the hydrodynamic loading and response evaluation that need to be performed. Potential and viscous effects on the FSO/FPSO come into play equally important role on the acting flow around the ship hull. Furthermore, translational and rotational motions of the hull have to be incorporated all together into the analysis to produce a realistic picture of the physical problem.

Recently, Computational Fluid Dynamics (CFD) has been experiencing rapid advances due to both computer technology progress and efficient algorithms that have been developed to solve the Navier-Stokes (N-S) equations used in the flow analysis around ship hulls. The present work is a contribution to the numerical solution of the viscous flow around ship-like bodies.

In the present work, the slightly compressible Navier-Stokes equations (Wanderley et al. [15]) are solved through the conservative upwind TVD scheme of Roe [8] and Sweby [11]. This finite difference method is second order accurate in space and time. The physical domain is discretized using a Cartesian mesh and the no-slip boundary condition on the body surface is imposed through the Immersed Boundary Method (IBM), Vitola et al. [13]. The Cartesian mesh is not conformed to the body contour and the IBM is used to inform the fluid flow the presence of a body through a force field added to the momentum equations. The code was implemented using the message passing interface (MPI) and can be run in a cluster with an arbitrary number of computers. Numerical results were obtained for the

flows around a sphere without free surface and around a series-60 ship hull in order to verify the implemented code. The agreement between the numerical results and the experimental and numerical data from the literature indicates that the implemented code is able to reproduce correctly the drag coefficient, pressure field, velocity field, and the free-surface elevation around a ship hull.

2. Mathematical formulation

The slightly compressible Navier-Stokes equations written in 3-D Cartesian coordinates are given below in the conservative form with the volume fraction equation included.

$$Q_t + (E_e - E_v)_x + (F_e - F_v)_y + (G_e - G_v)_z = H \tag{1}$$

$$\rho = \rho_w c + \rho_{air}(1-c) \tag{2}$$

where

$$Q = \begin{Bmatrix} p \\ \rho u \\ \rho v \\ \rho w \\ c \end{Bmatrix}, \qquad H = \begin{Bmatrix} 0 \\ \rho \left(\frac{M_\infty}{F_n} \right)^2 h_x \\ \rho \left(\frac{M_\infty}{F_n} \right)^2 h_y \\ 0 \\ 0 \end{Bmatrix} \tag{3}$$

$$E_e = \begin{Bmatrix} pu \\ \rho u^2 + p \\ \rho vu \\ \rho wu \\ cu \end{Bmatrix} \quad G_e = \begin{Bmatrix} pw \\ \rho uw \\ \rho vw \\ \rho w^2 + p \\ cw \end{Bmatrix} \quad F_e = \begin{Bmatrix} pv \\ \rho uv \\ \rho v^2 + p \\ \rho wv \\ cv \end{Bmatrix} \tag{4}$$

$$E_v = \frac{M_\infty}{R_L} \begin{Bmatrix} 0 \\ u_x \\ v_x \\ w_x \\ 0 \end{Bmatrix} \quad G_v = \frac{M_\infty}{R_L} \begin{Bmatrix} 0 \\ u_z \\ v_z \\ w_z \\ 0 \end{Bmatrix} \quad F_v = \frac{M_\infty}{R_L} \begin{Bmatrix} 0 \\ u_y \\ v_y \\ w_y \\ 0 \end{Bmatrix} \tag{5}$$

Equation (1) is solved numerically together with the initial conditions (6), boundary conditions on the body surface (7), and free-stream boundary conditions (8), where M_∞=0.2 for incompressible flows, and β=1 (water) and β=0 (air).

Initial conditions:

$$\begin{cases} p = 1 \\ u = M_\infty \\ v = 0 \\ w = 0 \\ c = \beta \end{cases} \tag{6}$$

Boundary conditions on the body surface:

$$\begin{cases} \partial p / \partial n = 0 \\ u = 0 \\ v = 0 \\ w = 0 \\ \partial c / \partial n = 0 \end{cases} \tag{7}$$

Free stream boundary conditions:

$$\begin{cases} p = 1 \\ u = M\infty \\ v = 0 \\ w = 0 \\ c = \beta \end{cases} \tag{8}$$

3. Numerical formulation

Equation (9) shows the conservative scheme used to solve the governing equations. The second order Lax-Wendroff method is used for the time integration, and the spatial derivatives are approximated using second order finite differences.

$$\begin{aligned} Q_{i,j}^{n+1} = Q_{i,j}^{n} - \Delta t \Big[& \delta_\xi E_e + \delta_\eta F_e + \delta_\zeta G_e - \\ & \nabla_\xi E_v - \nabla_\eta F_v - \nabla_\zeta G_v - \\ & \nabla_\xi E_{RS} - \nabla_\eta F_{RS} - \nabla_\zeta G_{RS} - H \Big]^n \end{aligned} \tag{9}$$

The Roe – Sweby fluxes are responsible for the upwinding and TVD of the scheme, see Eq. (10). For more details about the application of the upwind TVD scheme of Roe –Sweby to the slightly compressible Navier-Stokes equations, refer to Wanderley et al. [15].

$$\left(E_{RS}\right)_{i+1/2,j} = \frac{1}{2}\tilde{A}_{i+1/2,j}\left(Q_{i+1,j}^{n} - Q_{i,j}^{n}\right) \tag{10}$$

where

$$\tilde{A} = T\tilde{\Lambda}T^{-1} \tag{11}$$

In Eq. (11), the matrix $\tilde{\Lambda}$ is a diagonal matrix with terms shown in Eq. (12) and the matrix T is defined in Eq. (13).

$$\tilde{\lambda}_k = |\lambda_k| + \psi_k \left[\frac{\Delta t}{\Delta x} |\lambda_k|^2 - |\lambda_k| \right] \tag{12}$$

$$T = \left[\vec{x}_1, \vec{x}_2, \vec{x}_3, \ldots, \vec{x}_k \right] \tag{13}$$

where $(\lambda_k, \vec{x}_k)$ are the eigenvectors and eigenvalues of the Jacobian matrix A defined in Eq. (14).

$$A = \frac{\partial E_e}{\partial Q} \tag{14}$$

The van Leer [12] flux limiter defined in Eq. (15) is a function of the coefficient r defined in Eq. (16) in the wave domain.

$$\psi_k = \begin{cases} 0 & r_k \le 0 \\ \dfrac{2r_k}{1+r_k} & r_k > 0 \end{cases} \tag{15}$$

$$r_k = \begin{cases} \dfrac{w^k_{i+2,j} - w^k_{i+1,j}}{w^k_{i+1,j} - w^k_{i,j}} & \lambda_k \le 0 \\ \dfrac{w^k_{i,j} - w^k_{i-1,j}}{w^k_{i+1,j} - w^k_{i,j}} & \lambda_k > 0 \end{cases} \tag{16}$$

where

$$\vec{w} = T^{-1}\vec{Q} \tag{17}$$

The no-slip boundary condition on the body surface is imposed using the Immersed Boundary Method (IBM), Vitola et al. [13]. In this method, the flow field is informed of the body presence through a force field added to the momentum equations. These forces are computed such that the no-slip condition on the body surface is satisfied. The forces are applied only on the grid points close to the body surface through the reconstruction of the flow properties by linear interpolation. Fig. 1 illustrates the geometry of interpolation.
The properties of the flow field at the pyramid base (grid points 1, 2, and 3) are known because those are computed by the solver. The property at the pyramid pick (point 0 at the body surface) is imposed such that the no-slip condition on the body surface is satisfied. For example, the force added to the x-momentum equation (at point R) is computed as shown in Eq. (18). In this equation, u_R is the reconstructed velocity and u is the velocity obtained by the solver in the iterative process.

$$F_x = \rho \frac{u_R - u}{\Delta t} \tag{18}$$

where

$$u_R = ax_R + by_R + cz_R + d \tag{19}$$

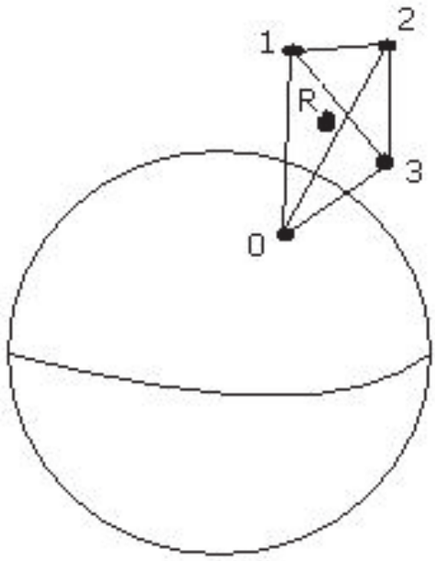

Fig. 1. Reconstruction geometry.

The coefficients a, b, c and d in Eq. (19) are obtained by the solution of the system of linear equations shown in Eq. (20).

$$\begin{aligned} ax_1 + by_1 + cz_1 + d &= u_1 \\ ax_2 + by_2 + cz_2 + d &= u_2 \\ ax_3 + by_3 + cz_3 + d &= u_3 \\ ax_0 + by_0 + cz_0 + d &= u_0 \end{aligned} \tag{20}$$

where u_0=0 is the no-slip condition on the body surface.

4. Grid generation

A Cartesian computational mesh generator is used to discretize the three-dimensional physical domain. The grid is refined in the region close to the body to allow the capturing of viscous effects close to the body surface. An exponential stretching is used to concentrate grid points close to the body surface and to coarsening the computational mesh in regions away from the body, where the variation of the flow properties is small. The Cartesian computational mesh does not fit the body surface and the no-slip boundary condition is imposed using the Immersed Boundary Method (IBM). Fig. 2 shows a computational mesh plane at the level of the undisturbed free surface. The grid is divided in slices and each slice is superimposed to the neighbors such that the boundary of one side corresponds to interior points of the other. Each slice is solved by different nodes in the computer cluster using the message passing interface (MPI). Between successive iterations, the slices communicate to the neighbors for boundary condition update.

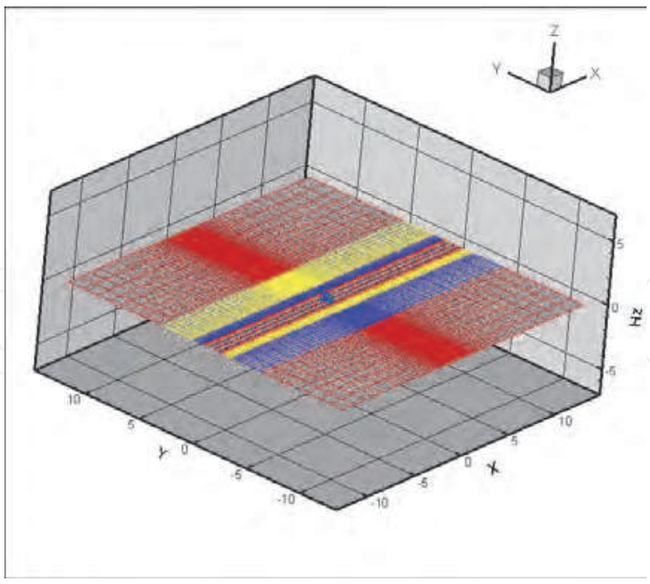

Fig. 2. Computational mesh.

5. Flow field around a sphere without free surface

The results obtained for the flow field around a sphere without free surface are presented below.

Figure 3 presents the pressure field and stream lines around a sphere. The figure shows two vortices attached to the trailing edge of the body, the stagnation point (in red) at the leading edge, and two regions of low pressure (in blue) at the top and bottom of the sphere. This result agrees with what is observed experimentally. For Reynolds number equal to 200, two vortices attached to the trailing edge of the sphere are observed experimentally.

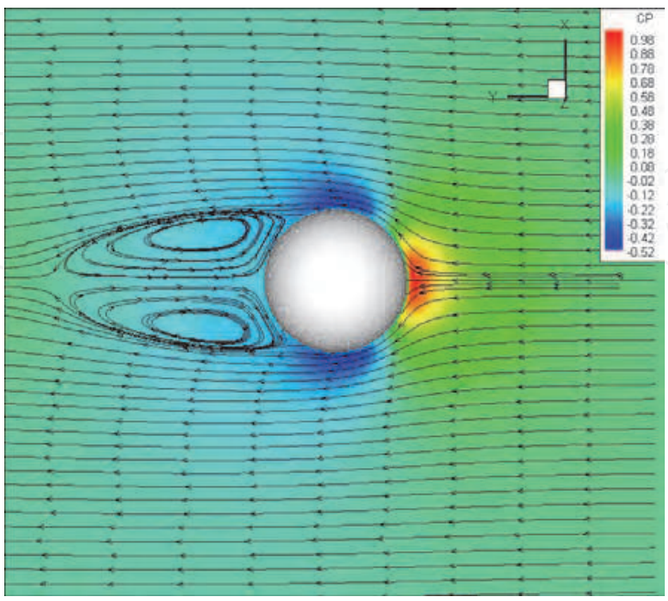

Fig. 3. Pressure field and stream lines around a sphere for *Re*=200.

Figure 4 presents the temporal series of the total drag (in black), frictional drag (in blue), and pressure drag (in red) coefficients for the sphere for Reynolds number equal to 200. Table 1 presents a comparison between the total drag coefficient obtained in the present work and other experimental and numerical data obtained from the literature. The agreement among the three results is remarkable.

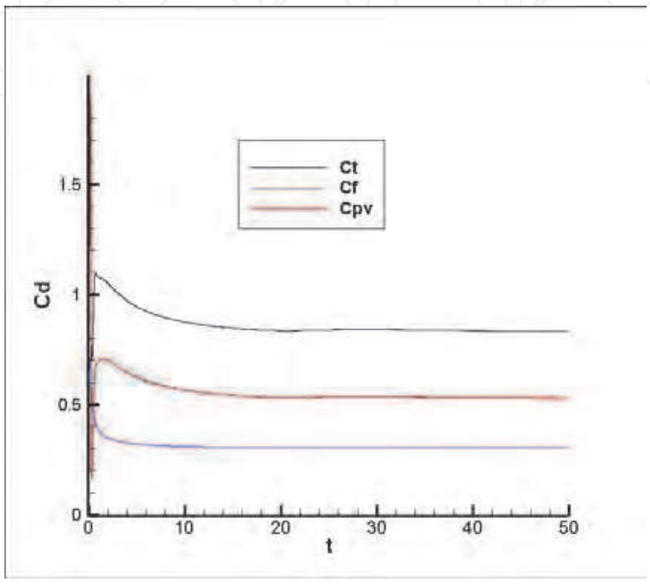

Fig. 4. Frictional, pressure, and total drag coefficients for *Re*=200.

Reference	*Re*	*Ct*	Comment
Schlichting [10]	100 200	1.100 0.800	Experimental
Campregher [2]	100 200	1.178 0.815	Numerical
Present study	100 200	1.200 0.832	Numerical

Table 1. Comparison of drag coefficient comparison.

6. Flow field around a series-60 hull

Additional verification of the numerical code is presented for the Series-60 hull for a low Reynolds number of 1.0×10^3. Figures 5, 6, and 7 show a plane of the computational grid generated around the hull at the level of the undisturbed free surface. The grid has 240x160x160 points and the smallest element is a cube with dimension of 0.0075Lpp. The grid has 11Lpp in the y direction, and 7.2 Lpp in the x and z directions.

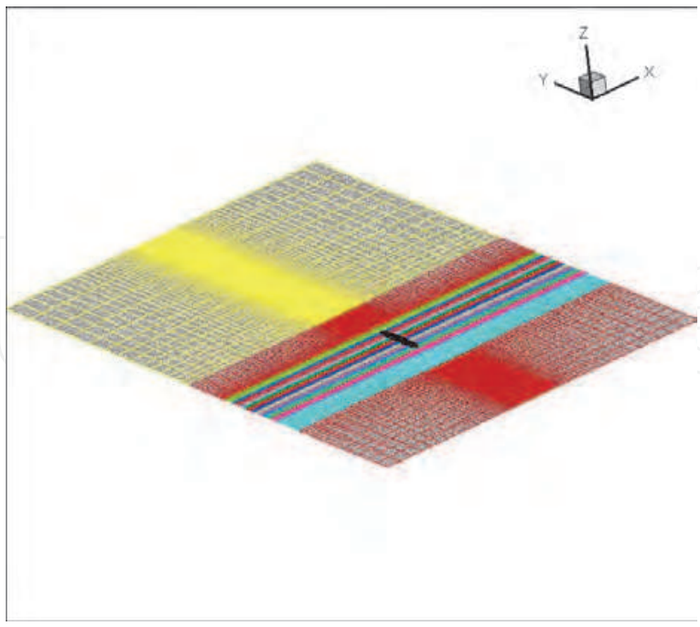

Fig. 5. Grid generated around the Series-60 hull.

A top view and a bottom view of the hull can be seen in Fig. 6 and Fig. 7, respectively. Close to the body, the grid is uniform and sufficiently refined to capture the viscous effects close to the hull surface. An exponential stretching is used to increase the size of the grid elements away from the body, where property gradients are small.

Fig. 6. Grid generated around the Series-60 hull (top view).

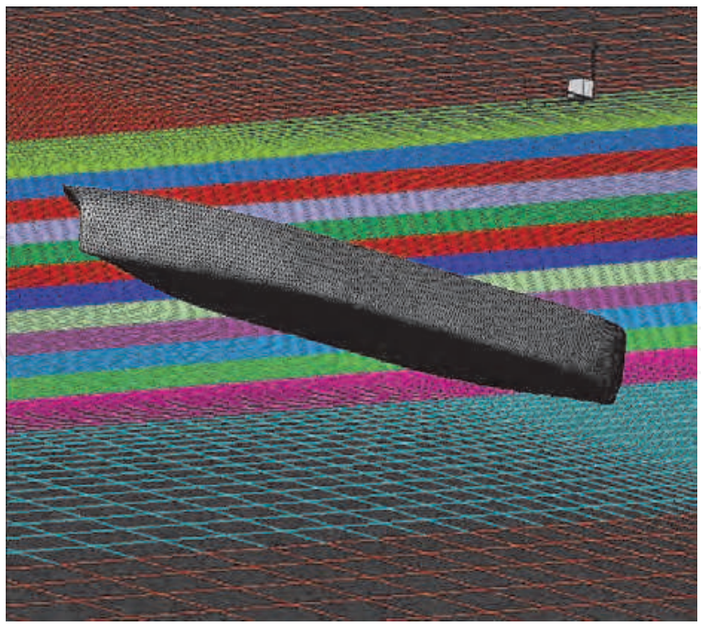

Fig. 7. Grid generated around the Series-60 hull (bottom view).

Figure 8 illustrates the pressure contour around the Series-60 hull at the same plane of the undisturbed free-surface. In this simulation, the free-surface is not allowed to deform. A stagnation point (in red) is observed at the bow of the hull and a low pressure region (in blue) is observed at the side walls of the body.

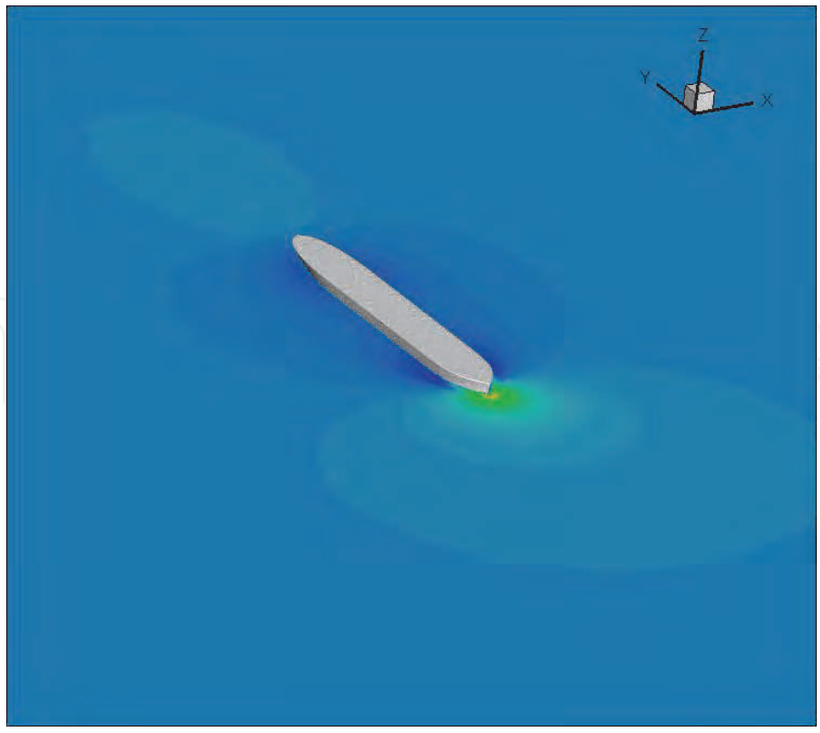

Fig. 8. Pressure field around the series-60 hull, R_L=1.0x10^3, Fn=0.25.

Figure 9 illustrates the pressure contour and the velocity field around the hull. The velocity profile inside the boundary layer and at the wake can be observed at the body surface and behind the hull, respectively.

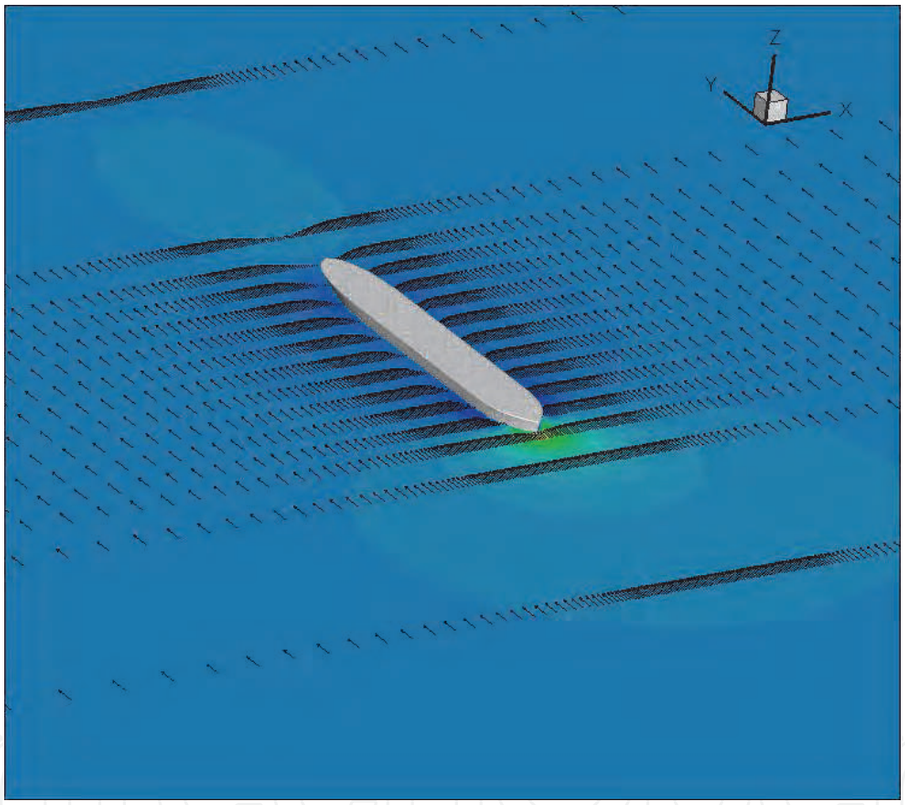

Fig. 9. Pressure and velocity fields around the Series-60 hull, R_L=1.0x10^3, Fn=0.25.

Figure 10 shows the free surface elevation after allowing the free surface to deform and after the steady state is obtained. The diverging wave formation can be observed at the port and starboard of the ship hull. Figure 11 shows the velocity field around the hull and at the level of the free surface. The velocity profile inside the boundary layer along the side walls of the hull and at the wake of the body can be observed in yellow arrows.

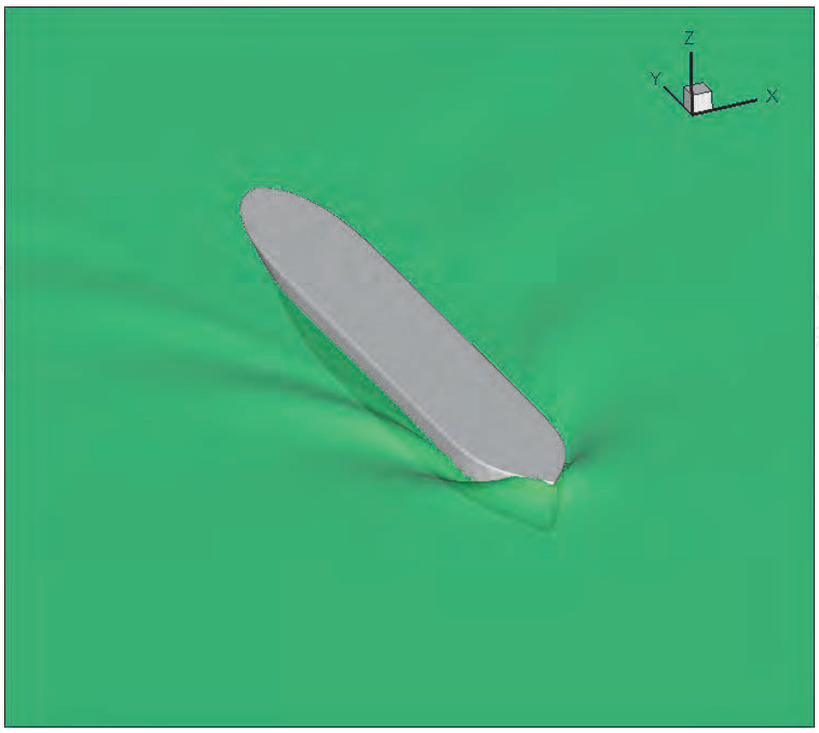

Fig. 10. Free-surface elevation around the Series-60 hull, R_L=1.0x10^3, Fn=0.25.

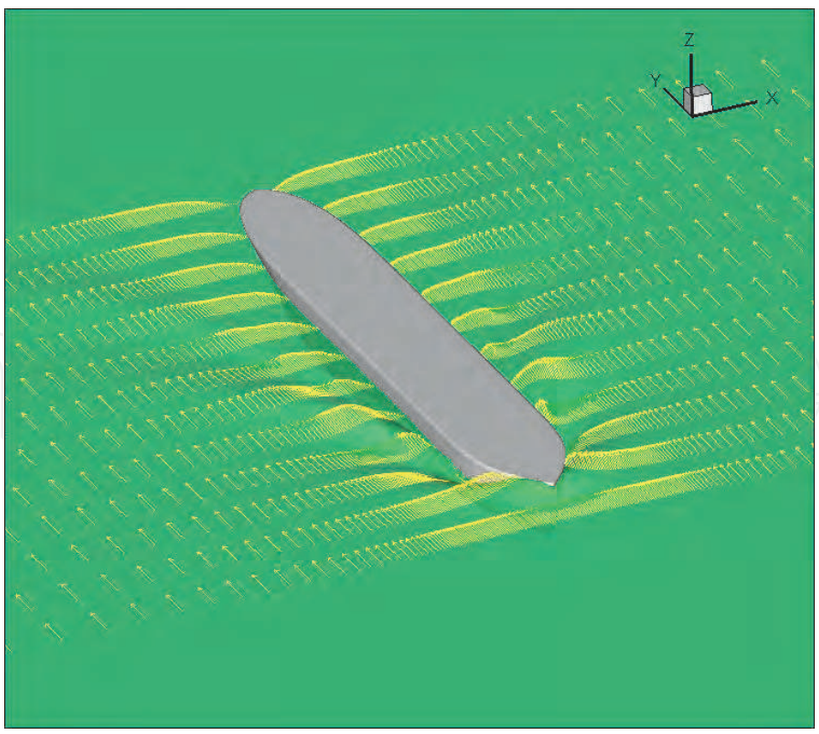

Fig. 11. Free-surface elevation around the Series-60 hull, R_L=1.0x10^3, Fn=0.25 and velocity field.

Figure 12 presents the pressure coefficient contour around the ship hull at the level of the free surface. The low pressure regions can be seen in blue at the wave crests of the divergence wave and the high pressure regions can be seen in red at the bow of the ship and at the wave trough.

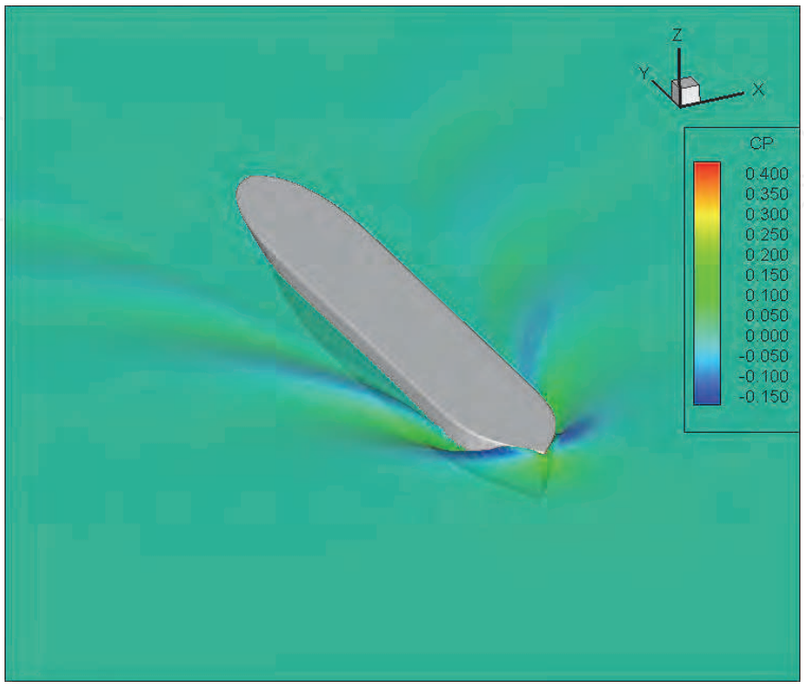

Fig. 12. Free-surface elevation around the Series-60 hull, R_L=1.0x10^3, Fn=0.25 and pressure field.

Figure 13 shows the total (in red), frictional (in black), and pressure (in blue) drag coefficients on the ship hull. After time=4, the steady state is obtained and the drag coefficients are constant.

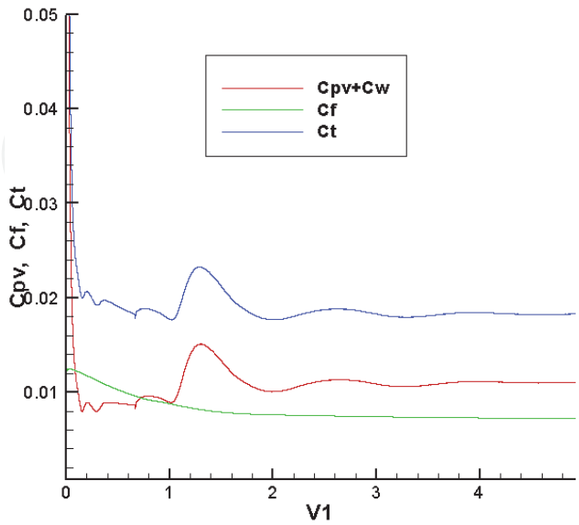

Fig. 13. Drag coefficient on the Series-60 hull, R_L=1.0x10^3, Fn=0.25.

7. Conclusions

An upwind and TVD numerical scheme was implemented to solve the unsteady slightly compressible Navier-Stokes equations for the free-surface flow around ship hulls. The physical domain is discretized in a Cartesian grid and the boundary condition on the body surface is implemented using the Immersed Boundary Method (IBM).

The implemented code is parallelized using MPI to be run in an arbitrary number of computers of a cluster. The numerical code was verified for the flow around a sphere, and a Series-60 hull.

The results obtained for the sphere were compared to numerical and experimental data from literature showing the good quality of the numerical results. The numerical results obtained for the ship hull were not compared to other numerical and experimental data because of the difficulty to find those data for lower Reynolds number. However, the numerical results agree qualitatively well to experiments.

Next phase of development will include the implementation of the k-ε turbulence model and validation of the numerical code for higher Reynolds numbers and configurations of practical interest, such as, resistance to motion, moonpool – free decay and forced motion, wave run-up and air gap, and wake and shadow flows.

8. Acknowledgments

This research was sponsored by the Brazilian Innovation Agency – FINEP under Grant 0106067200.

9. References

[1] Alessandrini, B., and Delhommeau, G., 1994, "Simulation of Three-Dimensional Unsteady Viscous Free Surface Flow around a Ship Model", International Journal for Numerical Methods in Fluids, Vol. 19, pp.321-342.

[2] Campregher, R., Mansur, S. S., and Silveira-Neto, A., 2005, "Numerical Simulation of the Flow Around a Sphere Using the Immersed Boundary Method for Low Reynolds Number", Proceedings of the Sixth International ERCOFTAC Workshop on Direct and Large-Eddy Simulation, held at the University of Poitiers, September, 12-14.

[3] Ciortan, C., Wanderley, J., and Guedes, C., 2007, "Turbulent Free-surface Flow around a Wigley Hull Using the Slightly Compressible Formulation", Ocean Engineering, V. 34, pp. 1383-1392.

[4] Ciortan, C., Guedes, C., and Wanderley, J., 2007, "Assessment of Free Surface Treatment Techniques and Turbulence Models Influence Using the Slightly Compressible Flow Simulation", Proceedings of the 26th International Conference on Offshore Mechanics and Arctic Engineering, June 10-15, San Diego, California, USA.

[5] Hino, T., 1987, "Numerical Simulation of a Viscous Flow with a Free Surface around a Ship Model", Journal of the Society of Naval Architects of Japan, Vol. 161.

[6] Ratcliffe, T., 1998, "Validation of the Free Surface Reynolds-Averaged navier-Stokes and Potential Flow Codes", Proceedings of the 22nd ONR Symposium on Naval Hydrodynamics.

[7] Rider, W.J., and Kothe, D. B., 1997, "Reconstructing Volume Tracking", Journal of Computational Physics, Vol. 141, 112-152.

[8] Roe, P. L., 1984, "Generalized Formulation of TVD Lax-Wendroff Scheme, ICASE Report 84-53.

[9] Rudman, M., 1997, "Volume-Tracking Methods for Interfacial Flow Calculations", International Journal for Numerical methods in Fluids, Vol. 24, 671-691.

[10] Schlichting, H., 1979, "Boundary Layer Theory". McGraw-Hill, New York.

[11] Sweby, P. K., 1984, "High Resolution Scheme Using Flux Limiter for Hyperbolic Conservation Laws, SIAM J. Num. Anal., vol. 21, pp. 995-1011.

[12] van Leer, B., 1979, "Towards the Ultimate Conservative Difference Scheme, V: A Second-Order Sequel to Godunov's Method, J. Comput. Phys., vol. 32, pp. 101-136.

[13] Vitola, M. A., Schettini, E. B. C., and Silvestrini, J. H., 2006, "Three Dimensional Wake Structure of Free Planar Shear Flow Around Horizontal Cylinder". In: Eric Lamballais, Rainer Friedrich, Bernard J. Geurts and Olivier Métais. (Org.). Direct and Large-Eddy Simulation VI. : Springer Netherlands, 2006, p. 669-676.

[14] Wanderley, J. B. V., and Levi, C., 2006, "Free Surface Viscous Flow around a Ship Model", Proceedings of the 25th International Conference on Offshore Mechanics and Arctic Engineering, June 4-9, Hamburg, Germany.

[15] Wanderley, J. B. V., Souza, G. H. B., Sphaier, S. H., and Levi, C. A., 2008, "Vortex-Induced Vibration of an Elastically Mounted Circular Cylinder using an Upwind TVD Two-Dimensional Numerical Scheme", Ocean Engineering, V. 35, pp. 1533-1544.

Computational Simulations and Applications

Edited by Dr. Jianping Zhu

ISBN 978-953-307-430-6
Hard cover, 560 pages
Publisher InTech
Published online 26, October, 2011
Published in print edition October, 2011

The purpose of this book is to introduce researchers and graduate students to a broad range of applications of computational simulations, with a particular emphasis on those involving computational fluid dynamics (CFD) simulations. The book is divided into three parts: Part I covers some basic research topics and development in numerical algorithms for CFD simulations, including Reynolds stress transport modeling, central difference schemes for convection-diffusion equations, and flow simulations involving simple geometries such as a flat plate or a vertical channel. Part II covers a variety of important applications in which CFD simulations play a crucial role, including combustion process and automobile engine design, fluid heat exchange, airborne contaminant dispersion over buildings and atmospheric flow around a re-entry capsule, gas-solid two phase flow in long pipes, free surface flow around a ship hull, and hydrodynamic analysis of electrochemical cells. Part III covers applications of non-CFD based computational simulations, including atmospheric optical communications, climate system simulations, porous media flow, combustion, solidification, and sound field simulations for optimal acoustic effects.

InTech Europe
University Campus STeP Ri
Slavka Krautzeka 83/A
51000 Rijeka, Croatia
Phone: +385 (51) 770 447
Fax: +385 (51) 686 166
www.intechopen.com

InTech China
Unit 405, Office Block, Hotel Equatorial Shanghai
No.65, Yan An Road (West), Shanghai, 200040, China
中国上海市延安西路65号上海国际贵都大饭店办公楼405单元
Phone: +86-21-62489820
Fax: +86-21-62489821

IntechOpen